J Therm Anal Calorim (2014) 116:321–328
DOI 10.1007/s10973-013-3565-6

Thermal stability and conductivity of hot-pressed Si_3N_4–graphene composites

P. Rutkowski · L. Stobierski · G. Górny

Received: 16 October 2013 / Accepted: 25 November 2013 / Published online: 10 December 2013

Abstract This study concerns new Si_3N_4–graphene composites manufactured using the hot-pressing method. Because of future applications of silicon nitride for cutting tools or specific parts of various devices having contact with high temperatures there is a need to find a ceramic composite material with good mechanical and especially thermal properties. Excellent thermal properties in the major directions are characteristic of graphene. In this study, the graphene phase is added to the silicon nitride phase in a quantity of up to 10 mass%, and the materials are sintered under uniaxial pressure. The mixture of AlN and Y_2O_3 is added as sintering activator to the composite matrix. The studies focus on thermal stability of produced composites in argon and air conditions up to the temperature of 1,000 °C. The research also concerns the influence of applied uniaxial pressure during the sintering process on the orientation of graphene nanoparticles in the Si_3N_4 matrix. The study also presents research on anisotropy of thermal diffusivity and following thermal conductivity of ceramic matrix composites versus the increasing graphene quantity. Most of the presented results have not been published in the literature yet.

Keywords Silicon nitride · Graphene · Microstructure · Thermal stability · Thermal conductivity

P. Rutkowski (✉) · L. Stobierski · G. Górny
Department of Ceramics and Refractories, Faculty of Materials Science and Ceramics, AGH University of Science and Technology, al. Mickiewicza 30, 30-059 Kraków, Poland
e-mail: pawelr@agh.edu.pl; Pawel.Rutkowski@agh.edu.pl

Introduction

Polycrystalline pure silicon nitride shows good mechanical properties, such as bending strength, fracture toughness or abrasion wear, and oxidation resistance at higher temperatures [1–3]. It is the reason why this material is used for cutting tools bearing balls and other parts of devices working in heavy conditions [4–6]. For these applications, except mechanical properties, the material should be characterized by good thermal conductivity to remove the heat quickly from the working zone and should be easily mechanically treated to prepare sometimes very complicated parts of devices. From this point of view Si_3N_4-sintered body shows thermal conductivity of approx. 30 W/mK [7] (which is not very high) and is very resistant to mechanical treatment [8].

The addition of graphene can help to solve this problem [9]. This phase shows in a major crystallographic direction very good thermal and electrical properties [8, 10–12]. So there is hope that doping the silicon nitride materials by the graphene phase can lead to an increase in thermal conductivity and the electrical one, which can allow the materials to be shaped by electro-discharge machining. Because of low strength of the interphase boundaries between silicon nitride and graphene, too high an addition of this phase can change the mechanical properties of the composite—but it can be solved by manufacturing gradient materials. Almost, all the research on the Si_3N_4–graphen system concerns the mechanical and tribological properties [13–16]. The author of this study did not found any literature containing data on thermal stability and thermal conductivity of silicon nitride–graphene composites, which is very important from the point of view of the application.

This study concerns a new approach to silicon nitride–graphene composites, where the graphene is added up to 10 mass%. The materials are sintered by hot-pressing,

where the applied uniaxial pressure can influence the distribution of graphene in the silicon nitride matrix. That is why the studies are focused on the anisotropy of microstructure and following it the anisotropy of thermal diffusivity/conductivity, which has not been found in the literature. Because of possible high temperature applications of the material, the thermal stability in various atmospheres is determined. The studies also show the dilatometric measurements on thermal expansion coefficient (CTE) in perpendicular direction to the load applied during the sintering, which can be very important for designing multilayer or gradient materials.

Experimental materials and methods

Si_3N_4–graphene composites were prepared from major commercial powders: submicron silicon nitride (0.5–0.8 μm) Grade M11 of H.C. Starck and graphene (GNP, 550 nm average particle, 8 nm of flake thickness) Grade AO-2 of Graphene Laboratories. To activate the sintering the aluminum nitride (0.8–1.8 μm) Grade C of H.C. Starck and yttria (0.5–0.8 μm) Grade C of H.C. Starck were used. They were added to the Si_3N_4 matrix initial powder in the following quantities: 2.5 mass% AlN and 4 mass% Y_2O_3. The powders were blended to obtain mixtures containing 0, 0.5, 1, 2, 4, 6, 8, and 10 mass% of the graphene phase. The sets prepared in this way were subjected to the homogenization process using a rotary–vibratory mill. The preparation step was made in an environment of isopropyl alcohol for 6 h at 80 % chamber filling using silicon nitride-milling balls. Such a high filling of the milling chamber was aimed at dispersing well and

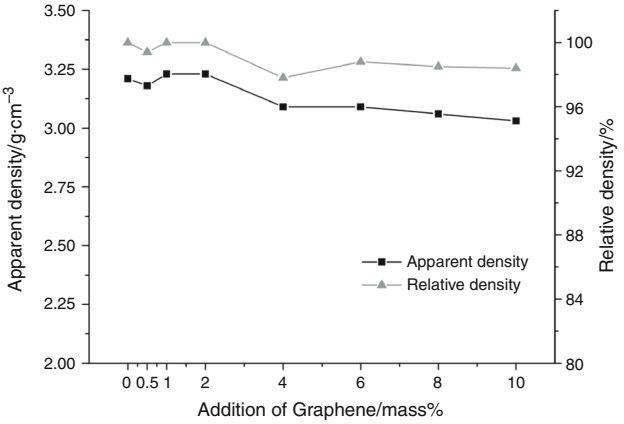

Fig. 1 Density of Si_3N_4–graphene composites

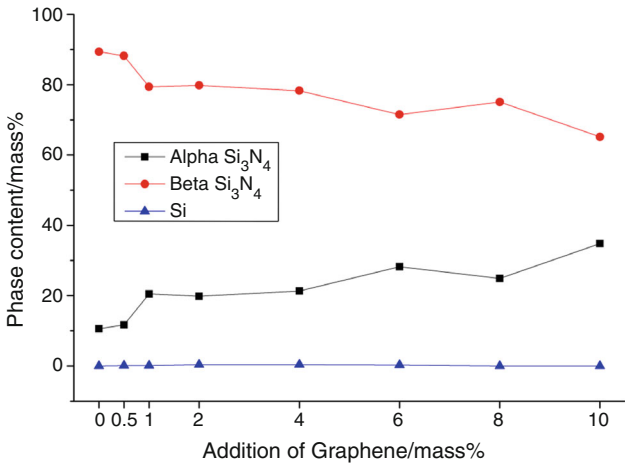

Fig. 2 Phase analysis of Si_3N_4–graphene composites

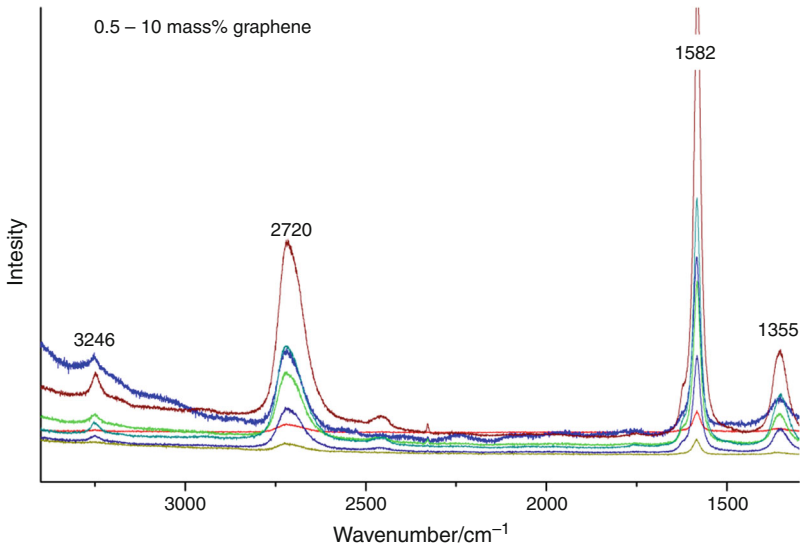

Fig. 3 Raman spectra analysis of Si_3N_4–graphene composites

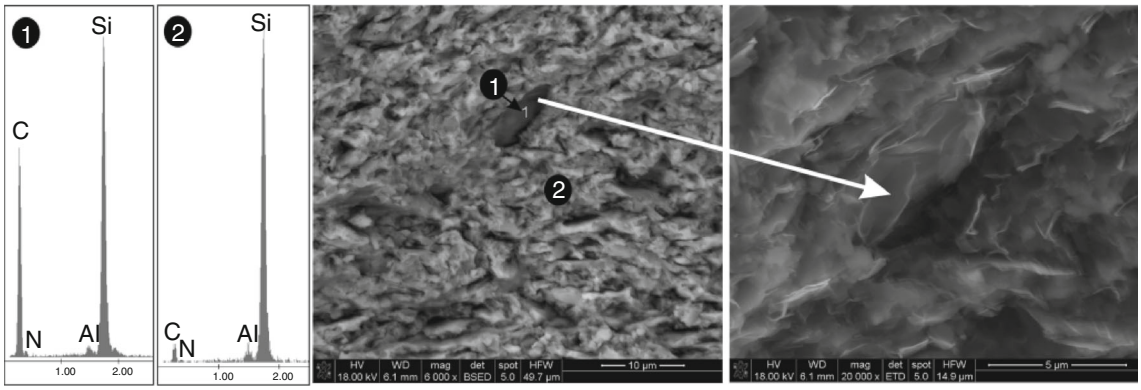

Fig. 4 Point element distribution of Si_3N_4–10 mass% graphene composites

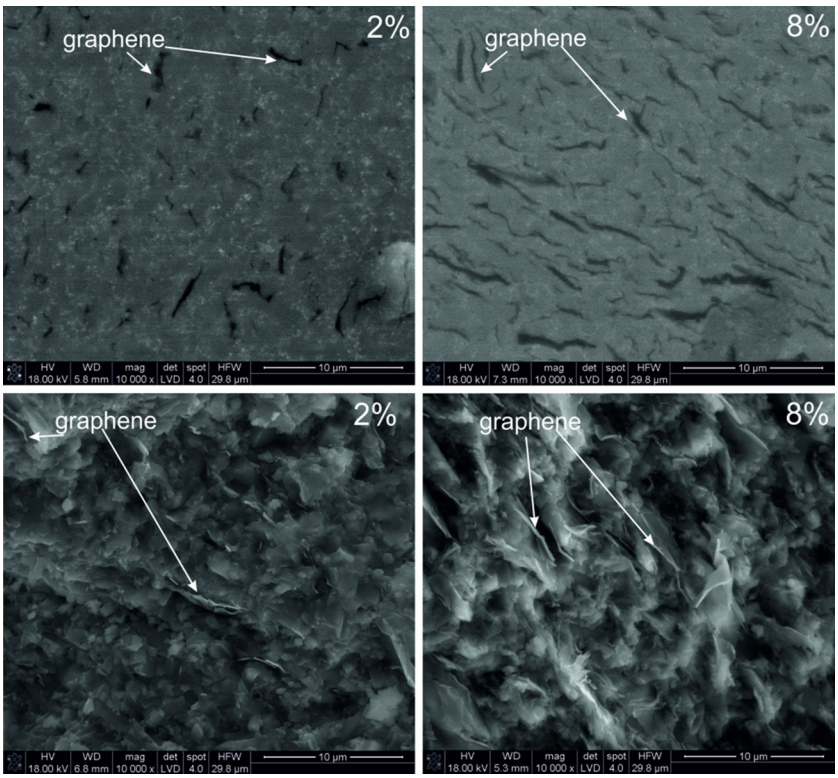

Fig. 5 Microstructure of Si_3N_4–graphene composites

destroying graphene agglomerates. After the drying and granulation process, the mixtures were hot-pressed by a HP apparatus of Thermal Technology INC. The sintering under uniaxial pressing was carried out in a nitrogen flow under pressure of 25 MPa with a 10 °C/min heating rate up to a temperature of 1,750 °C. The samples were held at the maximum sintering temperature for 60 min. Sintered bodies with a diameter of 50 mm were obtained.

The apparent density measurements of sintered composites were made by means of a hydrostatic method, and then the relative density was calculated. The Si_3N_4–graphene samples were polished in the direction perpendicular to the pressing axis of the HP-sintering process. The material surfaces prepared in this way were subjected to XRD phase analysis and then the content of alpha and beta Si_3N_4 phases was determined. The identification of the graphene phase was performed by Raman spectroscopy (Horriba Yvon Jobin LabRAM HR micro-Raman spectrometer equipped with a CCD detector). The microstructural observation of surfaces and fractures of Si_3N_4–graphene composites was conducted by means of scanning electron microscopy (SEM). The examination of point element deposition of silica and carbon was performed using the EDS method.

The thermal stability was measured in argon and air flow by means of thermogravimetric TG measurements using STA 449 F3 Jupiter®. The gases analysis in the air during heating up the sample containing graphene was performed

by STA 449 F3 Jupiter® with quadrupole mass spectrometer (QMS).

Heat measurements were performed on a Netzsch LFA 427 apparatus. To determine the specific heat by comparative method, Pyroceram 9606 reference material, with the known coefficient of thermal expansion and specific heat, was used. Thermal diffusivity was determined using the laser pulse method (LFA) for the reference and test material at temperatures ranging from 25 to 700 °C in argon flow, using the "Cape-Lehmann + pulse correction" computational model. At each temperature, three measurements were performed for statistical purposes. Examination of tested materials density changes as a function of temperature in the range up to 900 °C was performed by determining the coefficient of thermal expansion using a Netzsch DIL 402C dilatometer. Based on these measurements, specific heat was determined using the following formula:

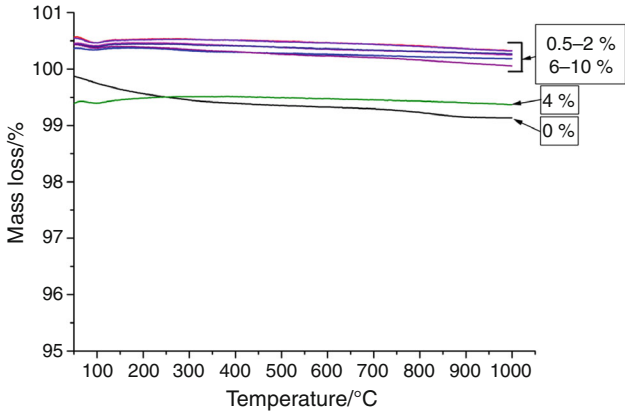

Fig. 6 Thermal stability of Si_3N_4–graphene composites in the argon atmosphere

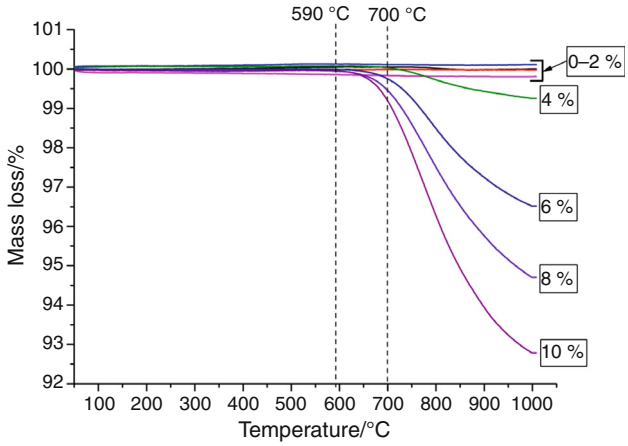

Fig. 7 Thermal stability of Si_3N_4–graphene composites in the air atmosphere

$$c_p^{\text{sample}} = \frac{T_\infty^{\text{ref}}}{T_\infty^{\text{sample}}} \cdot \frac{Q^{\text{sample}}}{Q^{\text{ref}}} \cdot \frac{V^{\text{sample}}}{V^{\text{ref}}} \cdot \frac{\rho^{\text{ref}} \cdot D^{\text{ref}}}{\rho^{\text{sample}} \cdot D^{\text{sample}}} \cdot \frac{d^{2,\text{sample}}_{\text{orifice}}}{d^{2,\text{ref}}_{\text{orificer}}} \cdot c_p^{\text{ref}} \quad (1)$$

where c_p specific heat of the sample/reference (J g^{-1} K^{-1}), T temperature of the sample/reference (K), Q energy absorbed by the sample/reference (J), V amplitude of signal gain for the sample/reference, ρ apparent density of the sample/reference (g cm^{-3}), D thickness of the test material (mm), d diameter of the measuring aperture of the sample/reference (mm).

The thermal conductivity was calculated from the following equation:

$$\lambda(T) = a(T) \cdot c_p(T) \cdot \rho(T) \quad (2)$$

where $a(T)$ thermal diffusivity (mm^2 s^{-1}), c_p (T) specific heat (J g^{-1} K^{-1}), $\rho(T)$ density of the material (g cm^{-3}).

Results and discussion

The results of hydrostatically measured apparent density and calculated relative density are presented in Fig. 1.

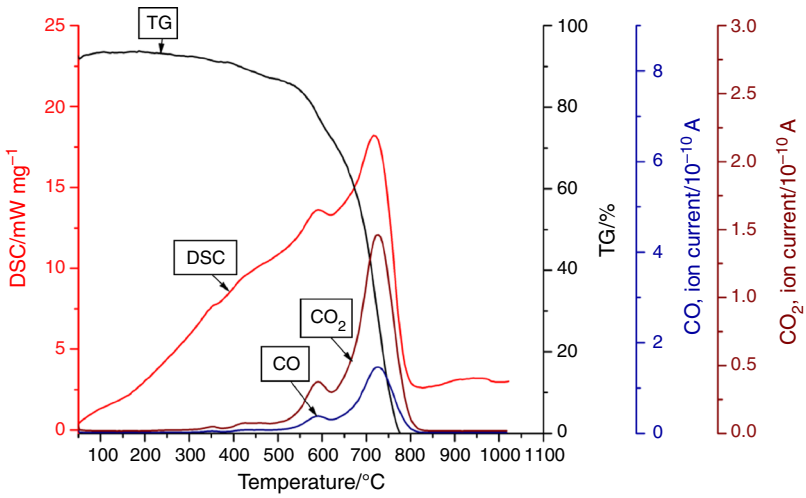

Fig. 8 QMS gas mass analysis of graphene in the air atmosphere

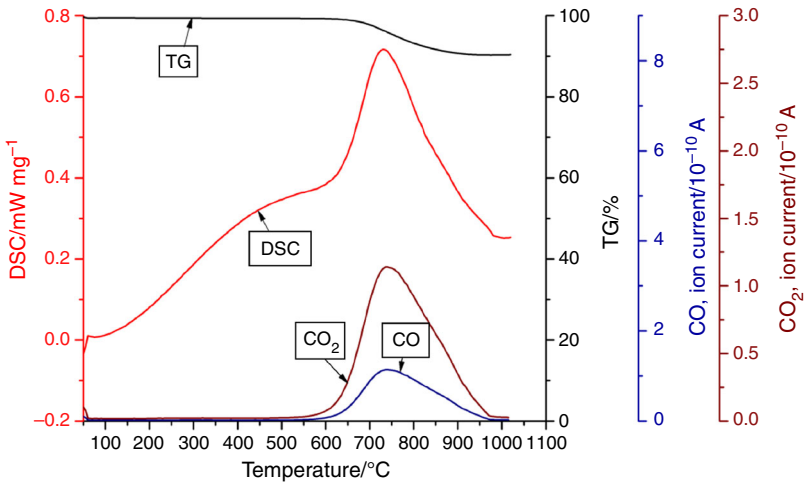

Fig. 9 QMS gas mass analysis of Si_3N_4–10 mass% graphene composite in the air atmosphere

Table 1 The value of thermal expansion coefficient (CTE) of Si_3N_4–graphene system

Composition	CTE (120–800 °C) × 10^{-6}/°C^{-1}
Si_3N_4	3.32
Si_3N_4 + 0.5 mass% graphene	3.23
Si_3N_4 + 1 mass% graphene	3.01
Si_3N_4 + 2 mass% graphene	3.31
Si_3N_4 + 4 mass% graphene	3.08
Si_3N_4 + 6 mass% graphene	3.21
Si_3N_4 + 8 mass% graphene	3.08
Si_3N_4 + 10 mass% graphene	2.97

The results show that hot-pressed Si_3N_4–graphene composites are well densified, and the relative density is above 98 % of theoretical density. The results of the matrix XRD phase analysis of manufactured materials are illustrated in Fig. 2 and the identification of graphene by Raman spectroscopy is shown in Fig. 3.

The results of phase analysis (Figs. 1, 2) show that two alpha and beta phases exist in the composites' matrix and there are very small amounts of free silica. The addition of graphene leads to an increase in the beta silicon nitride content. The Raman spectroscopy analysis performed confirms the presence of graphene in the all prepared composites. The wavenumbers of pure graphene powder are: 3243, 2727, 1578, and 1349 cm^{-1}.

The results of EDS point element distribution and the images of the surface and fractures of some of the manufactured composites are shown in Figs. 4 and 5.

The point EDS analysis of silica and carbon distribution also confirms the presence of the graphene phase in the materials, which is visible in Fig. 4 as thin layers. The

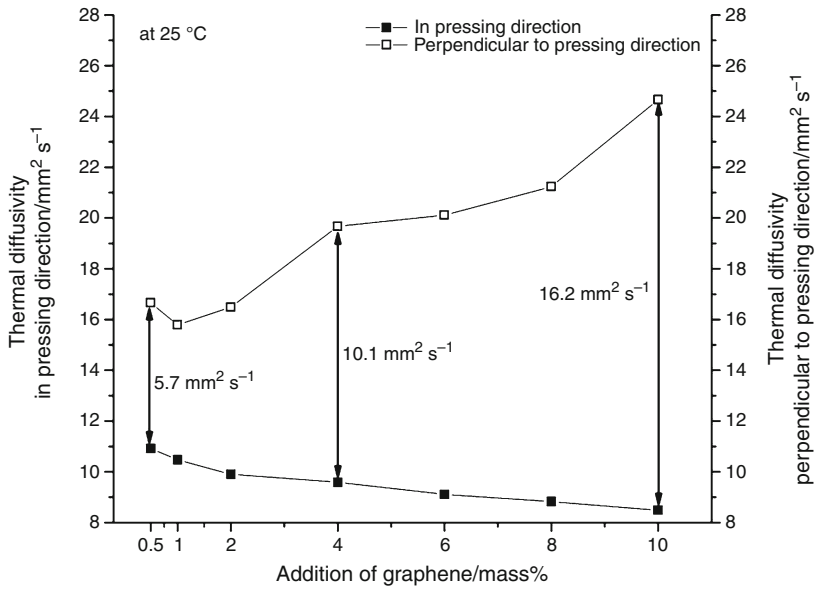

Fig. 10 Difference in thermal diffusivity of Si_3N_4–graphene composites at temperature of 25 °C

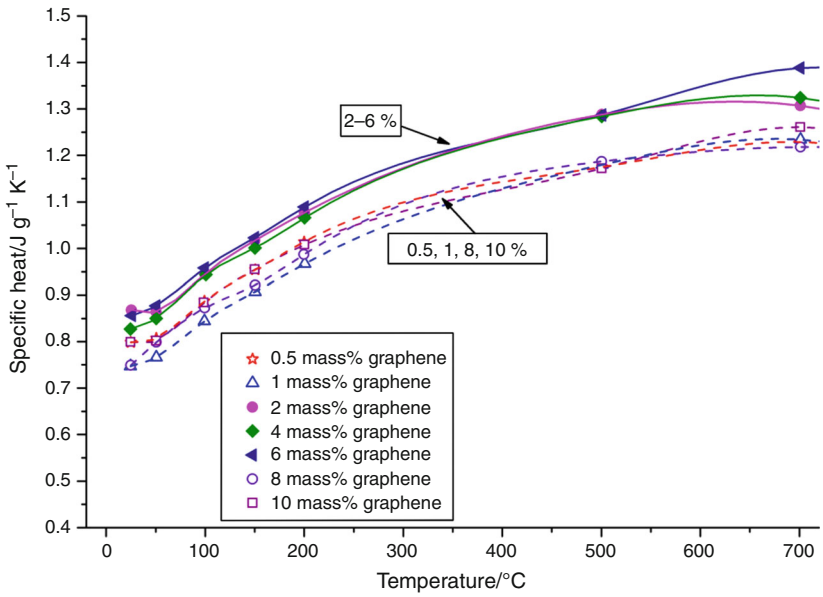

Fig. 11 Specific heat of Si_3N_4–graphene composites

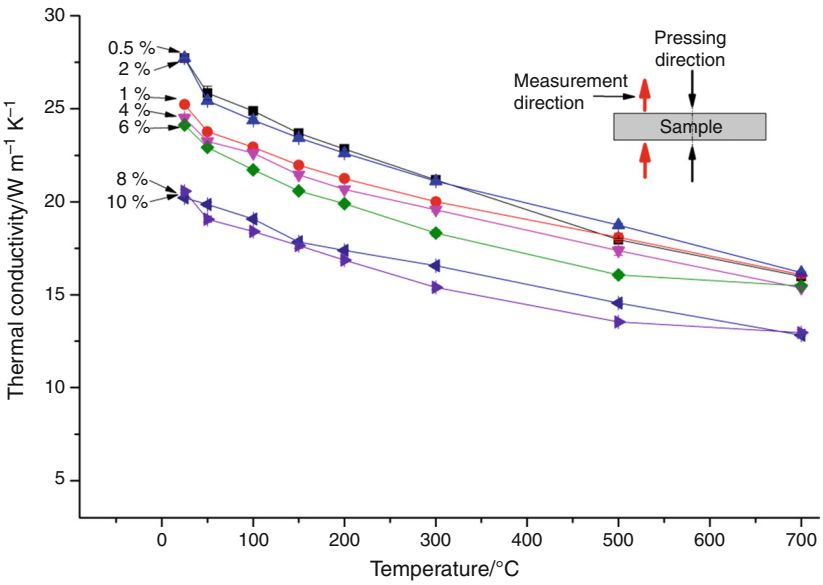

Fig. 12 Thermal conductivity of Si_3N_4–graphene composites in the pressing direction

aluminum comes from the activating sintering process. Further observations made on the material surface indicate graphene particles orientation in the direction perpendicular to the pressing axis during the sintering (Fig. 5). This situation is similar to the h-BN orientation in hot-pressed Al_2O_3/h-BN composites [17]. It can have a very important influence on thermal conductivity of the composites, which will be presented in this study. The white mist is probably the effect of material charging during the SEM observation.

The thermal stability measurement of the sintered Si_3N_4–graphene composites was made in argon and in air atmosphere up to 1,000 °C, and the results of thermogravimetric and mass gas analysis are shown in Figs. 6–9.

The results of thermogravimetric measurements show that all the prepared composites are stable at least up to the temperature of 1,000 °C in a protective atmosphere (Fig. 6). The thermal stability of the Si_3N_4–graphene materials in case of the air atmosphere depends on the content of the graphene phase (Fig. 7). For composites containing up to the 2 mass% of graphene the material is totally stable (no mass change) up to the temperature of 1,000 °C—the silicon nitride matrix protects the graphene phase from oxidation. Also, for 4 mass% graphene the mass lost is very small and it starts at 700 °C. The beginning of graphene oxidation process shifts with the increasing C content to 600 °C for 10 mass% of the graphene additive, and the loss of the mass increases significantly.

The gas mass (QMS) analysis shows that the oxidation of pure graphene starts even below 500 °C (Fig. 8). In the case

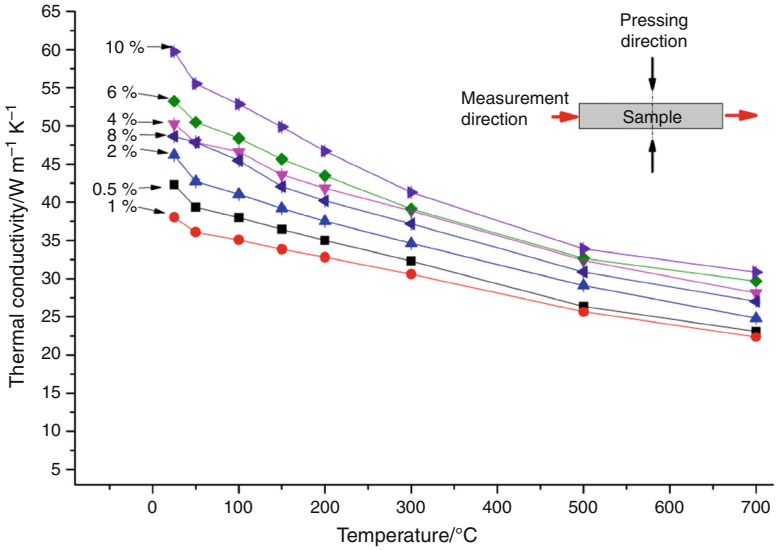

Fig. 13 Thermal conductivity of Si_3N_4–graphene composites perpendicular to the pressing direction

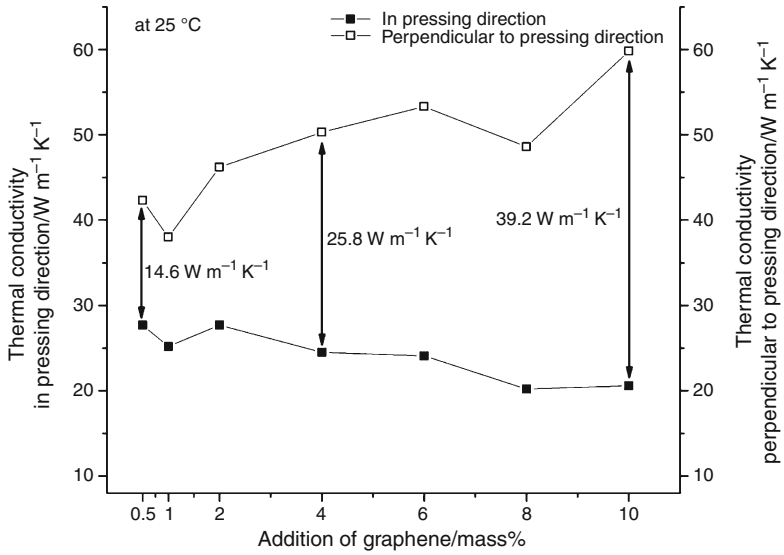

Fig. 14 Difference in thermal conductivity of Si_3N_4–graphene composites

of sample containing 10 mass% of graphene the oxidation of composite dispersed phase begins at 600 °C when the change of the material mass and the evolved gas signal is recorded. The QMS analysis confirms the TG measurements.

From the point of view of further possible applications, for example, for gradient composites the thermal expansion coefficient is very important. The CTE values of dilatometric measurements, made in the direction perpendicular to the sintering pressing axis are collected in Table 1. The results show that the addition of the graphene phase does not change the CTE value significantly.

From the side of the graphene application to the ceramic materials, it is important to check if it has any influence on heat transfer of the produced composites. The values of direct measurements of thermal diffusivity made using the laser flash analysis method in two different directions are illustrated in Fig. 10. The thermal diffusivity was also measured up to 600 °C for determination of thermal conductivity versus temperature (Figs. 12, 13).

The results of the measurements show that the addition of graphene to the silicon nitride matrix leads to a decrease in thermal diffusivity in the pressing direction (uniaxial pressing during the hot-pressing process). In accordance with the microstructure (Fig. 5), the thermal examinations indicate that the thermal diffusivity increases strongly with the increasing addition of graphene in the perpendicular direction to the pressing axis. The anisotropy of thermal diffusivity, measured at 25 °C in the different directions, is presented in Fig. 10 and reaches even 190 % for the sample containing 10 mass% of the graphene phase. Thermal diffusivity results in Fig. 10 confirms the microstructural observations of oriented graphene particles.

Figure 11 illustrates the specific heat measured by laser flash analysis method. The c_p values for materials containing

graphene are slightly higher than for silicon nitride (approx. 0.7 in literature) for sample 2–6 mass% of graphene, for other manufactured materials it is almost the same.

The directly measured thermal diffusivity, density changes (CTE changes), and the determined specific heat allowed for calculating the thermal conductivity of the obtained Si_3N_4–graphene composites. The results of thermal conductivity for a different direction in the material in function of temperature and its comparison (anisotropy) at 25 °C are shown in Figs. 12, 13, and 14.

Also, like in the case of thermal diffusivity, generally, the thermal conductivity decreases by 30 % in the pressing direction (during the hot-pressing process) with an increasing graphene content (Fig. 12). In the perpendicular direction, the thermal conductivity increases with an increase in the graphene addition by about two times for the case of 10 mass% graphene (Fig. 13). The results at 25 °C presented in Fig. 14 indicate anisotropy from 53 % for 0.5 mass% graphene to 190 % for 10 mass% graphene. The thermal conductivity results confirm microstructural observations of oriented graphene particles.

Conclusions

- The hot-pressing allows for obtaining well-densified Si_3N_4–graphene materials. The microstructural observations show that the use of uniaxial pressing during the sintering process leads to the graphene orientation in the perpendicular direction to the pressing axis.
- The Raman spectra analysis and EDS analysis with microstructural observations confirm the presence of graphene in the Si_3N_4 matrix. The XRD phase analysis shows that the content of beta silicon nitride increase with the addition of graphene.
- The composites with graphene addition up to 4 % are well thermally stable in air atmosphere.
- The microstructural anisotropy of graphene in silicon nitride matrix is reflected in the anisotropy of thermal diffusivity and thermal conductivity that reaches even 190 %.
- The thermal expansion coefficient does not change significantly in all composites in the function of graphene addition in the direction perpendicular to the pressing axis, which is important in the case of gradient Si_3N_4–graphene materials production.

Acknowledgements The study constitutes a part of the project "Ceramic composites with graphene content as cutting tools and device parts with unique properties No. GRAF-TECH/NCBR/03/05/2012. The authors thank very much Dr. Janusz Partyka from AGH University of Science and Technology for the QMS analysis.

References

1. Hampshire S. Silicon nitride ceramics—review of structure, processing and properties. J Achiev Mater Manuf Eng. 2007;24:43–50.
2. Zhang Y-W, Yu J-B, Xia Y-F, Zuo K-H, Yao D-X, Zeng Y-P, Ren Z-M. Microstructure and mechanical performance of silicon nitride ceramics with seeds addition. J Inorg Mater. 2012;27:807–12.
3. Švec P, Brusilová A, Kozánková J. Effect of microstructure and mechanical properties on wear resistance of silicon nitride ceramics. Mater Eng. 2008;16:34–40.
4. Klemm H. Silicon nitride for high-temperature applications. J Am Ceram Soc. 2010;93:1501–22.
5. O'brien MJ, Presser N, Robinson EY. Failure analysis of three Si_3N_4 balls used in hybrid bearings, Aerospace Report no. TR-2003(8565)-1, Engineering and Technology Group, The Aerospace Corporation, 2003
6. Ariff TF, Shafie NS, Zahir ZM. Wear analysis of silicon nitride (Si_3N_4) cutting tool in dry machining of T6061 aluminum alloy. Appl Mech Mater. 2013;268–270:563–7.
7. Kim HS, Park S-Y, Hur BY, Lee SW. Mechanical and thermal properties of silicon nitride hot pressed with adding rare-earth oxides. Mater Sci Forum. 2005;486–487:181–4.
8. Lee J, Lim S, Shin D, Sohn H, Kim J, Kim J. Laser assisted machining process of HIPed silicon nitride. JLMN-J Laser Micro/Nanoeng. 2009;4:207–11.
9. Geim AK, Novoselov KS. The rise of graphene. Nat Mat. 2007;6:183–91.
10. Wonbong C, Lee J-W. Graphene: synthesis and applications. Boca Raton: CRC Press; 2012.
11. Warner JH, Schaffel F, Bachmatiuk A, Rummeli MH. Graphene: fundamentals and emergent applications. Oxford : Elsevier; 2013.
12. Balandin AA, Ghosh S, Bao W, Calizo I, Teweldebrhan D, Miao F, Lau CN. Superior thermal conductivity of single-layer graphene. Nano Lett. 2008;8:902–7.
13. Hvizdoš P, Dusza J, Balázsi C. Tribological properties of Si_3N_4–graphene nanocomposites. J Eur Ceram Soc. 2013;33:2359–63.
14. Kvetkova L, Duszowa A, Kasiarova M, Dorcakova F, Dusza J, Balázsi C. Influence of processing on fracture toughness of Si_3N_4 + graphene platelet composites. J Eur Ceram Soc. 2013;33:2299–304.
15. Walker LS, Marotto VR, Rafiee MA, Koratkar N, Corral EL. Toughening in graphene ceramic composites. ACS Nano. 2011;5:3182–90.
16. Pfeifer J, Sáfrán G, Wéber F, Zsigmond V, Koszor O, Arató P, Balázsi C. Tribology study of silicon nitride-based nanocomposites with carbon additions. Mater Sci Forum. 2010;659:235–8.
17. Rutkowski P, Piekarczyk W, Stobierski L, Górny G. Anisotropy of elastic properties and thermal conductivity of Al_2O_3/h-BN composites. J Therm Anal Calorim. 2013. doi:10.1007/s10973-013-3246-5.